Electrochemical oxidation of binary copper-nickel alloys in cryolite melts

L. Cassayre[a,b], P. Chamelot[a], L. Arurault[c], L. Massot[a], P. Palau[b] and P. Taxil[a]

[a] Laboratoire de Génie Chimique (LGC) UMR CNRS 5503, Université Paul Sabatier, 118 route de Narbonne, 31062 Toulouse Cedex 04, France

[b] Alcan, Voreppe Research Center, 725 rue Aristide Berges, 38341 Voreppe, France

[c] Centre Interuniversitaire de Recherche et d'Ingénierie des Matériaux (CIRIMAT), UMR CNRS 5085, Université Paul Sabatier, 118 Route de Narbonne, 31062 Toulouse Cedex 09, France

Abstract: Anodic oxidation of copper, nickel and two copper-nickel alloys was studied in cryolite melts at 1000°C. In an oxide-free melt, anodic dissolution of each material was observed, and the dissolution potential increases with the content of copper. SEM characterization of a Cu55-Ni45 alloy showed that nickel is selectively dissolved according to a de-alloying process. In an alumina-containing melt, a partial passivation occurs at the copper-containing electrodes, at potentials below the oxygen evolution potential. A passive film forms on the copper electrode, while on the nickel electrode no dense oxide layer develops. Copper-nickel alloys were found to form a mixed oxide layer. At higher potentials, the formation of oxygen bubbles on the electrodes results in a degradation of the passive films and a strong corrosion.

Keywords: molten salts (A), copper nickel alloys (A), selective oxidation (C), passive films (C), de-alloying (C)

1

1. Introduction

The search for an inert anode material to be used in primary aluminium production is aimed at replacing the consumable carbon anode in order to achieve the following cell reaction:

$$Al_2O_{3(dissolved)} = 2\ Al_{(liquid)} + 3/2\ O_{2(gaz)} \tag{1}$$
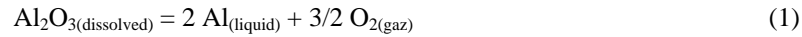
Among the required properties for the anode material, the stability under strong oxidative conditions (oxygen atmosphere, at 1000°C, in a corrosive fluoride melt composed mainly of cryolite Na_3AlF_6) is one of the more difficult to achieve.

Many materials have been developed for this application [1], and a cermet, consisting of a nickel ferrite-nickel oxide substrate containing a copper-nickel alloy as metal phase, is considered as one of the most promising. However, it has been observed [2, 3] that the metal phase of this ceramic-metal composite tends to oxidize and dissolve in the molten salt.

Pure metal phases have also been studied to be used as anodes in cryolite melts. For instance, Tarcy [4] investigated on the behaviour of iron, copper and nickel by cyclic and linear voltammetry. Hryn and Sadoway [5] performed electrolysis of alloys containing aluminium. Recently, Shi et al. [6] published results concerning the behaviour of Cu-Ni superalloys in electrolytes having lower melting points (750-850°C).

In most cases, these studies were focused on determining the corrosion rates of the anodes and/or the current efficiencies obtained, relatively to aluminium production. However, *ex situ* characterization of metal anodes after anodic polarizations are scarce, and the understanding of the corrosion mechanisms of alloys in cryolite melts has not been fully studied.

The present study is focused on determining which anodic reactions are taking place on copper-nickel alloys in cryolite melts. These alloys have been investigated for two main reasons. First, copper-nickel alloys are among the noblest metal phases in cryolite melts, and therefore were chosen as the metal phase of the most efficient cermets. Second, copper and nickel are totally miscible at 1000°C [7], so these alloys represent a good example of the behaviour of solid solutions used as anode in cryolite melts.

Two alloys (Cu70-Ni30 and Cu55-Ni45, in wt.%), pure copper and pure nickel were used as working electrodes for electrochemical characterization; then metal surface and corrosion products were analysed by the use of a microprobe.

In order to understand the role of oxides in the melt, anodic oxidation in a melt free of alumina was first investigated. Then, the oxidation process at potentials below oxygen evolution (E_{O2}=2.20 V vs. AlF$_3$/Al) and under electrolysis conditions (i=0.8 A/cm^2) in a melt containing 5%wt. of alumina were determined.

2. Experimental

2.1 Cell

The cryolite melts were contained in a vitreous carbon crucible, placed in a graphite liner protecting the inside wall of a cylindrical vessel made of refractory steel. The cell was closed by a stainless steel lid cooled by circulating water. A scheme of the experimental setup has been presented elsewhere [8].

The atmosphere was U-grade (less than 5 ppm O_2) inert argon dehydrated with a purification cartridge (Air Liquide). An absolute pressure of around 1.3 bars was maintained during the runs.

2.2 Chemicals and bath preparation

Two compositions of cryolite melts were used: the first one without alumina and the second one containing alumina.

The alumina-free melt was composed of pure Na_3AlF_6 (Cerac, purity 99.5%), with an 11 wt.% excess of AlF$_3$ (Acros, purity 99.9+%) and 5 wt.% of CaF_2 (Merck, purity 99.95%), leading to a cryolite ratio (CR) of 2.2. The liquidus temperature was calculated to be 975°C [9].

The second melt had the same composition, with an addition of 5 wt.% of alumina. The liquidus temperature was then decreased to about 947 °C [9].

Two hundred grams of the mixture were placed in the cell, heated to 500°C and dehydrated under vacuum (10^{-5} bars) for 24 h. A temperature of 25°C above the melting point was maintained during electrochemical experiments, i.e. 1000°C concerning the alumina-free melt and 970°C for the alumina-containing melt. Careful electrolysis of the melt with low alumina content was performed for a few hours using a platinum electrode, in order to eliminate residual oxide species.

2.3 Electrodes

Metal wires of nickel, copper, and copper-nickel alloys with a diameter of 2 mm were supplied by Goodfellow. The composition of the alloys was 55 wt.% Cu – 45 wt.% Ni and 70 wt.% Cu – 30 wt.% Ni. These metals were used as working electrodes in a classic three-electrode setup and immersed 5-10 mm into the molten salt. The actual immersed height was determined at the end of the run.

The auxiliary electrode was an 8 mm diameter graphite rod (Carbone Lorraine).

Potentials were measured with respect to a platinum wire immersed in the bath and acting as a comparison electrode $Pt/PtO_x/O^{2-}$. The platinum electrode potential was calibrated to the aluminium deposition potential by measurement of its difference with the potential of a tungsten electrode on which aluminium was deposited by cathodic polarization [10].

2.4 Techniques and equipment

Electrochemical measurements were carried out using an Autolab PGSAT30 potentiostat controlled by GPES software. Three electrochemical techniques were used. Steady state current versus potential curves were recorded by applying a sweep rate of 0.002 V/s; short electrolysis at fixed potential allowed to plot the evolution of current with time; open-circuit potential of the working electrodes were recorded after anodic polarization.

Scanning electron microscope (SEM) observations were made on a LEO 435 VP. A microprobe Cameca Sx100 was used for copper-nickel alloys composition measurements.

3. Results and discussion

3.1 Anodic dissolution in alumina-free melts

3.1.1 Electrochemical study

Linear sweep voltammetry

Linear sweep voltammetry was performed on copper, nickel and both copper-nickel alloys in the oxide-free cryolite bath. The anodic potential was slowly increased (sweep rate 0.002 V/s) from the open circuit potential until high current densities, typically higher than 0.5 A/cm^2. The set of curves is presented in Fig. 1.

As it was shown in a previous paper [11], all metals undergo anodic dissolution in oxide-free cryolite melts. When the potential of the metal is kept below a particular value, E_M, typical of each metal investigated, the current density remains very low, indicating an absence of reaction at the electrode. Then, when the potential reaches E_M, the current density increases sharply with no limiting current.

Tafel slopes analysis indicates that the reactions are controlled by electronic transfer [11]. Furthermore, Fig. 1 shows that copper is more stable than nickel by about 0.35 V.

The behaviour of each alloy has been found to be intermediate between the pure metals: the values of the dissolution potentials of the alloys, reported in Table 1, are comprised between the dissolution potential of pure nickel and pure copper, and increases with the content of copper.

As reported by Pickering [12] from studies performed in aqueous media, the anodic current observed below the dissolution potential of pure copper should correspond only to the dissolution of nickel.

Electrolysis at constant potential

Potensiostatic polarizations of the electrodes were performed in the oxide-free cryolite melt. The imposed potential values were chosen at overpotentials of about 0.30 - 0.35 V compared to the dissolution potentials of each metal or alloy.

Fig. 2 exhibits the evolution of current density with time, plotted on a logarithmic scale, for the oxidation of copper, nickel and copper-nickel 55-45. For the pure metals, current density is found to remain stable over the duration of the run, indicating that no passivation of the metal occurs. According to a subsequent SEM analysis of a cross-section of the electrodes (not shown here), it was confirmed that no passivation layer has formed.

In the case of the copper-nickel 55-45 electrode polarized at E=1.80 V vs. AlF_3/Al, a significant decrease of the current density was observed during the first 10-20 seconds of the run. This is attributed to a selective dissolution of nickel nearby the surface of the alloy, and is confirmed by the structural analysis of the alloy surface presented below. Then, the dissolution occurs at a constant current density.

A potentiostatic polarization of the copper-nickel 55-45 alloy was also performed at E=1.45 V vs. AlF_3/Al, just below the dissolution potential of the alloy measured on the linear voltammogram. The curve shown in Fig. 2 indicates that a reaction occurs at a current density of around 0.03 A/cm^2. Structural analysis of this electrode was performed in order to understand which reaction was taking place.

3.1.2 Structural and chemical analysis of copper-nickel alloy after anodic dissolution

The cross sections of two copper-nickel 55-45 electrodes were analysed after electrolysis at two different potentials.

The lower applied potential value (E=1.45 V vs. AlF$_3$/Al) was comprised between the dissolution potential of pure nickel and the potential of alloy dissolution, both measured on linear voltammograms.

The higher applied potential value (E=1.80 V vs. AlF$_3$/Al) was above the dissolution potential of both the alloy and pure copper.

Anodic dissolution at subcritical potentials

The cross section of the electrode polarized at E=1.45 V vs. AlF$_3$/Al (Fig. 3) exhibits a porous, 20-30 µm thick external layer. The optical observation evidences that this layer has the same colour as pure copper, whereas the bulk looks grey-metallic.

Microprobe analysis of the alloy surface was performed in order to measure the nickel and the copper atomic contents. Fig. 4a shows the microprobe data expressed by the copper molar fraction in the metal phase, while in Fig. 4b, a SEM-BSE micrograph indicates the part of the cross section which was analysed.

The microprobe analysis clearly shows that the porous layer is composed of almost pure copper: the alloy is nickel-depleted on a distance of about 30 µm from the surface. The specific dissolution of nickel is most likely limited by the diffusion of nickel from the bulk towards the surface of the alloy, which explains why the current density is low (~0.03 A/cm^2) during electrolysis.

Such a specific dissolution under the dissolution potential of the alloy has been widely studied in aqueous media [13, 14] and has been called *subcritical* dissolution. This term refers to the overall dissolution potential of the alloy and called *critical* potential. Due to the high temperature of operation in cryolite melts, the depth of the layer affected by the specific dissolution of the less stable element (here nickel) is larger by at least two orders of magnitude compared to aqueous media.

Furthermore, the morphology of the layer (large porosities dispersed in a nearly pure copper layer) is typical of the de-alloying of single phase binary alloys. The pattern formation has for instance been studied on Au-Ag alloys in aqueous media [15].

Congruent dissolution

After an electrolysis run of 800 s at E=1.80 V vs. AlF$_3$/Al in the oxide-free melt, the electrode diameter has strongly reduced due to the dissolution of the alloy. Observation of the cross section of the electrode by optical microscopy (Fig. 5) shows that only a very thin external layer (less than 10 µm) is depleted in nickel. This has been confirmed by microprobe analysis of the surface.

At this potential, which is above the dissolution potential of pure copper, nickel and copper dissolve congruently.

3.2 Alumina-containing melts

3.2.1 Electrochemical study

Linear sweep voltammetry

Plotting of steady state current versus potential were recorded at a scan rate of 0.002 V/s on nickel, copper and copper-nickel electrodes in the cryolite melt containing 5 wt.% of alumina. This technique was used to compare the potentials at which each metals oxidises to the potential of oxygen evolution E(O$_2$). In order to estimate the influence of the dissolved alumina on the oxidation reaction of the metals, the voltammograms were compared to those previously obtained in the oxide-free melt.

In the case of the nickel electrode (Fig. 6), the current density increases sharply and reaches 0.8 A/cm^2 at around 1.80 V vs. AlF$_3$/Al. According to Fig. 6, the metal oxidises at rate of around 2.3 A/cm² at the oxygen evolution potential, i.e. 2.20 V vs. AlF$_3$/Al. Nevertheless, the addition of alumina in the melt lowers a bit the rate of the oxidation reaction.

The oxidation of the copper electrode (Fig. 6) occurs at a potential more anodic than on nickel, and the reaction rate is significantly slower than in the oxide-free melt: the current density of the copper oxidation is about 0.3 A/cm^2 at 2.20 V vs. AlF$_3$/Al. This voltammogram is typical of a passivation process, which can be attributed to the growth of a low electronic-conductive oxide layer. However, the current density is still high in the potential range comprised between the beginning of the oxidation and the oxygen evolution, meaning that the oxidation of copper is still taking place at a quite high rate.

At a potential of 2.20 V vs. AlF$_3$/Al, a break in the curve indicates that the current associated to the oxygen evolution on the copper electrode participates to the overall process.

The oxidation of the copper-nickel 70-30 electrode (Fig. 7) occurs at a potential comprised between those of nickel and copper (~1.45 V vs. AlF$_3$/Al). The shape of the polarization curve is similar to the one observed on copper: (i) growth of a passivating layer on the alloy surface, limiting the current at less than 0.2 A/cm² below 2.20 V vs. AlF$_3$/Al, (ii) a sharp increase of current above 2.20 V vs. AlF$_3$/Al, due to oxygen evolution.

Potentiostatic polarization

Fig. 8 shows the variation of the current density with time during the potentiostatic polarization of the electrodes in each of the three investigated metals at 1.80 V vs. AlF$_3$/Al. At this potential, no oxygen evolution occurs, so the observed features are only due to the oxidation of the electrodes.

The current density at the nickel electrode is almost stable with time, confirming that no significant passivation of the electrode occurs. On the opposite, the copper electrode exhibits the typical behaviour of an electrode going through a passivation process: in a logarithmic scale, the current density decreases almost linearly with time. After 100 s, the current density tends to stabilize, which indicates that the passive film thickness becomes constant: a balance between the respective rates of oxide formation and dissolution takes place.

The copper nickel electrode exhibits an intermediate behaviour between pure nickel and pure copper electrodes: first, an active dissolution at high current densities, then a passivation process with a current decrease.

Open circuit potential recording

Evidence of the oxide layer formation on the electrodes after anodic polarization is confirmed by measuring the open circuit potential after a short anodic current pulse. As shown in Fig. 9, after a 5 s anodic polarization in the alumina containing melt, the copper electrode potential decreases to an intermediate value before decaying sharply to the rest value. This plateau is not observed in the case of the alumina-free melt and so corresponds to the equilibrium potential between copper and its oxide.

The plateaux observed during the open circuit potential recordings of each electrode, performed after anodic pulses, allow the potentials of oxide formation (Flade potential) to be measured accurately (Fig. 10). For pure copper and pure nickel, the measurements indicate $E_{ox(Ni)}$=1.40 V vs. AlF$_3$/Al and $E_{ox(Cu)}$=1.70 V vs. AlF$_3$/Al. In the case of the 70-30 copper-nickel alloy, several plateaux are observed in Fig. 10. The formation of several oxides is then assumed.

3.2.2 Structural and chemical analysis of surface layers

Analyses of the electrodes were first performed after electrolysis at potential below oxygen evolution, in order to examine the growth of the oxide layers in two potential ranges:

- below the oxygen evolution potential, so without the effect of oxygen,

- above the oxygen evolution potential, in order to study the influence of oxygen bubbling.

Characterization after potentiostatic polarization at potentials below oxygen evolution potential

SEM-BSE micrographs of the copper and the nickel electrodes after potentiostatic polarization at 1.80 V vs. AlF_3/Al are presented in Fig. 11.

Characterization of the nickel anode (Fig. 11a and 11b) indicates that no dense layer of nickel oxide has formed. Indeed, thin oxide layers (about 1 µm thick) detached from the surface and dissolved in a thick (over 100 µm) external layer mainly composed of salt. There is no clear explanation why this oxide layer did not grow to form a thick and dense layer, but it fit well with the potentiostatic measurements indicating that no passivation of the electrode occurred.

The micrographs 11c and 11d show that a thick and adherent oxide layer, composed of CuO according to EDX analysis, has grown on the surface of the copper electrode. This confirms the electrochemical study which pointed out a passivation process occurring on copper in this potential range.

The influence of the potential on the passivation process of a copper-nickel 70-30 electrode was studied by polarization at 1.50 V vs. AlF_3/Al and 1.80 V vs. AlF_3/Al.

After potentiostatic polarization at 1.50 V vs. AlF_3/Al, the SEM-BSE micrograph of a cross section of the electrode (Fig. 12a) does not show any thick oxide layer at the surface of the alloy. Microprobe analysis of nickel, copper and oxygen content, presented in Fig. 12b, indicates that only nickel has oxidized, since no copper is detected outside the alloy. The specific oxidation of nickel results in the formation of a few microns thick NiO layer at the surface of the alloy. Nickel is also present in the salt phase, most probably because of the dissolution of the oxide layer, as it was observed on pure nickel.

The observation of the copper-nickel electrode surface after polarisation at 1.80 V vs. AlF$_3$/Al reveals that a 50 µm thick oxide layer has formed. The molar fraction of copper in the alloy was determined close to the electrode-electrolyte interface by microprobe analysis: a depletion of nickel occurs only in a 10 µm depth. Microprobe analysis, shown in Fig. 13, allows establishing a quantitative map of nickel, copper, oxygen and aluminium distribution at the interface. The analysis indicates that the layer is composed of a mixture of copper, nickel and oxygen, but it was not possible to determine the composition of the oxide. It could be either a mixture of NiO, CuO or Cu$_2$O, or a mixed copper-nickel oxide (Cu, Ni)O. Anyhow, contrary to the pure nickel electrode, in this case the nickel oxide is retained in the oxide layer, and the presence of copper oxide prevents further nickel dissolution.

Furthermore, almost no aluminium was detected in this oxide layer, indicating that the layer is dense enough to prevent salt penetration.

Characterization after electrolysis at 0.8 A/cm^2

Oxygen evolution on nickel resulted in a fast dissolution of the electrode, with no adherent protecting layer, as already mentioned by Tarcy et al. [4].

In the case of copper and copper-nickel electrodes, when a current density of 0.8 A cm^{-2} was applied for 500 s, the oxide layer formed on the electrode surface was severely damaged by the oxygen bubbling, as illustrated in Fig. 14. It resulted in a noticeable corrosion of the electrodes. The corrosion rate, determined by measuring the diameter of the electrodes after several durations of electrolysis at 0.8 A/cm^2, can be estimated to be over 100 cm/yr both in the case of copper and copper-nickel. This is far over the limit of 1 cm/yr acceptable for an inert anode [16].

4. Conclusion

The study of the electrochemical oxidation of copper, nickel and copper-nickel electrodes in cryolite melts at 1000 °C allows proposing a degradation scheme of the copper-nickel alloys, depending on the applied potential and the alumina content.

In alumina-free melts, a specific dissolution of nickel occurs at potential below the dissolution potential of copper, resulting in characteristic de-alloying patterns. The typical size of the patterns is in the order of magnitude of 1 µm, which is 100 to 1000 times higher than what is reported in aqueous studies of Au-Ag or

Au-Cu de-alloying [12, 15]. This is attributed to the effect of high temperature and the subsequent increase of the interdiffusion coefficients.

In alumina-containing melts, the very first step of the degradation consists in a specific oxidation of the nickel contained in the alloy. No dense oxide layer forms on the alloy surface, but rather a very thin NiO layer which dissolves in the salt. The second step, occurring at higher potentials, is a congruent oxidation of the alloy, resulting in the growth of a dense mixed copper-nickel oxide at the surface. Then, under electrolysis condition (i=0.8 A/cm^2), the layer is damaged by oxygen bubbles, resulting in a fast corrosion of the electrodes. These results clearly confirm and explain previous studies showing that the copper-nickel phase of the cermet does not resist to corrosion when used as oxygen-evolving anodes for aluminium electrolysis.

Acknowledgements

References

[1] D.R. Sadoway, Inert anodes for the Hall-Héroult cell: The ultimate materials challenge, JOM- J. Min. Met. Mat. 53 (2001) 34-35.

[2] C.F. Windisch and S.C. Marschman, Electrochemical polarization studies on Cu and Cu-containing cermet anodes for the aluminum industry, Light Metals (1987) 351-355.

[3] E. Olsen and J. Thonstad, Nickel ferrite as inert anodes in aluminium electrolysis: Part II material performance and long-term testing, J. Appl. Electrochem. 29 (1999) 301-311.

[4] G.P. Tarcy, Corrosion and passivation of cermet inert anodes in cryolite-type electrolytes, Light Metals (1986) 309-320.

[5] J.N. Hryn and D.R. Sadoway, Cell testing of metal anodes for aluminum electrolysis, Light Metals (1993) 475-483.

[6] Z. Shi, J. Xu, Z. Qiu, B. Gao and Z. Wang, Copper-nickel superalloys as inert alloy anodes for aluminum electrolysis, JOM- J. Min. Met. Mat. 55 (2003) 63-65.

[7] T.B. Massalski, H. Okamoto, P.R. Subramanian and L. Kacprzak, Binary Alloy Phase Diagrams, 2nd ed., ASM International, Ohio, 1990.

[8] P. Chamelot, B. Lafage and P. Taxil, Studies of niobium electrocrystallization phenomena in molten fluorides, J. Electrochem. Soc. 143 (1996) 1570-1576.

[9] A. Solheim, S. Rolseth, E. Skybakmoen, L. Stoen, A. Sterten and T. Store, Liquidus temperatures for primary crystallization of cryolite in molten salt systems of interest for aluminum electrolysis, Metall. Mater. Trans. B 27b (1996) 739-744.

[10] W.E. Haupin, A scanning reference electrode for voltage contours in aluminum smelting cells, JOM- J. Min. Met. Mat. 23 (1971) 46-49.

[11] L. Cassayre, P. Chamelot, L. Arurault and P. Taxil, Anodic dissolution of metals in oxide-free cryolite melts, J. Appl. Electrochem. 35 (2005) 999-1004.

[12] H.W. Pickering, Characteristic features of alloy polarization curves, Corros. Sci. 23 (1983) 1107-1120.

[13] D. Landolt, Traité des matériaux : Corrosion et chimie de surface des métaux, Vol. 12, Presses polytechniques et universitaires romandes, Lausanne, 1993.

[14] J. Laurent and D. Landolt, Anodic dissolution of binary single phase alloys at subcritical potential, Electrochim. Acta 36 (1991) 49-58.

[15] J. Erlebacher and K. Sieradzki, Pattern formation during dealloying, Scripta Mater. 49 (2003) 991-996.

[16] U.S. Department of Energy, Inert anode roadmap, Report of The Aluminium Association Inc., http://www.eere.energy.gov/industry/aluminum/pdfs/inertroad.pdf (1998).

Legend of Figures

Figure 1:

Steady state current versus potential (0.002 V.s^{-1}) curves on copper, nickel, 70-30 and 55-45 copper-nickel alloys in the oxide-free cryolite melt [CR=2.2; 5%wt. CaF$_2$; T=1000 °C].
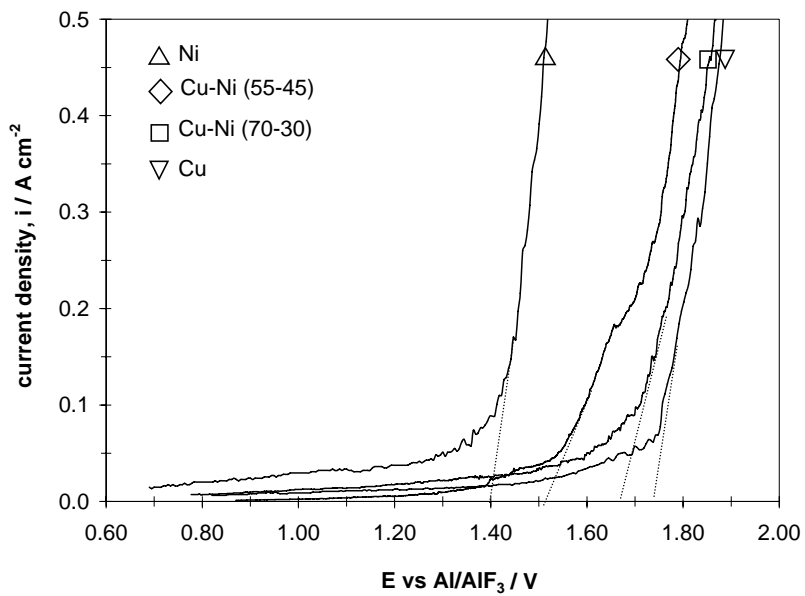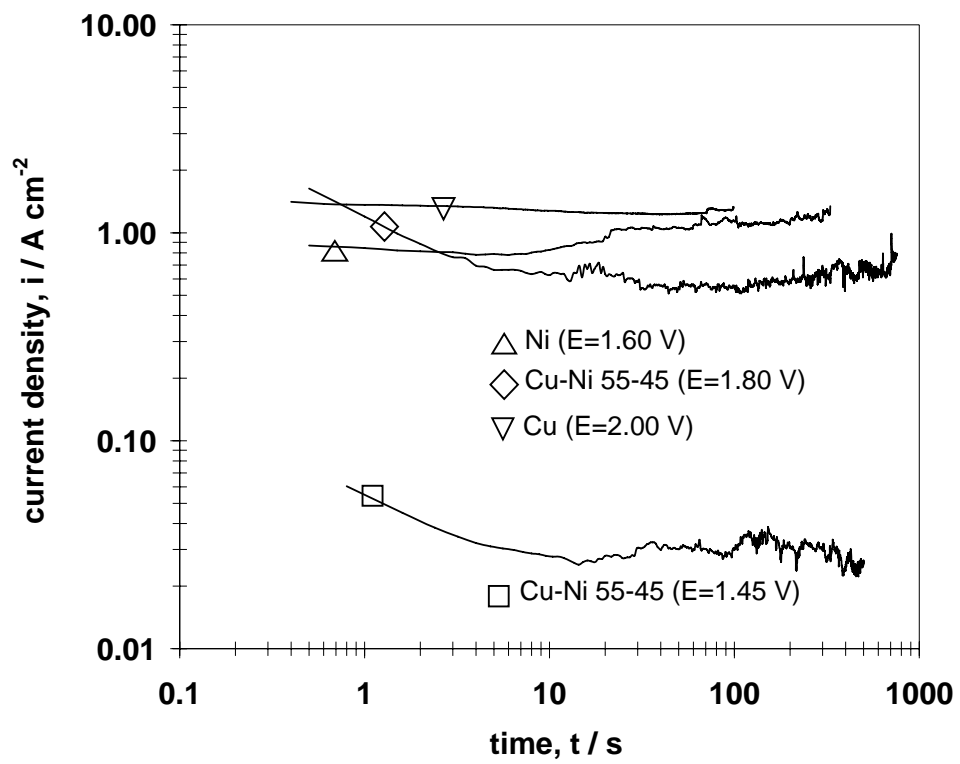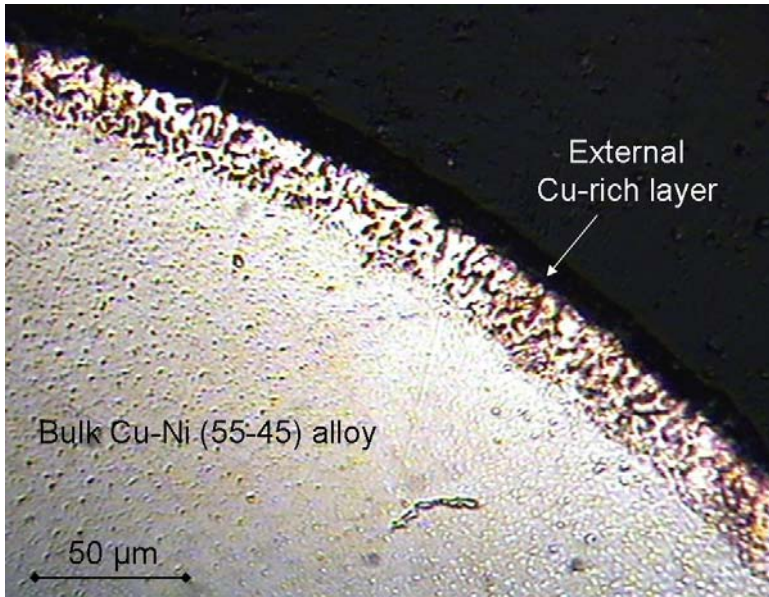
Figure 2:

Potentiostatic polarization on copper, nickel and copper-nickel 55-45 alloy in the oxide-free cryolite melt [CR=2.2; 5%wt. CaF$_2$; T=1000 °C].

Figure 3:

Optical micrograph of a cross section of the Cu-Ni 55-45 alloy after electrolysis at E=1.45 V vs. AlF$_3$/Al for 500 s in the oxide-free cryolite melt [CR=2.2; 5%wt. CaF$_2$; T=1000 °C].

Figure 4:

Chemical analysis of a cross section of the Cu-Ni 55-45 alloy after electrolysis at E=1.45 V vs. AlF$_3$/Al for 500 s in the oxide-free cryolite melt [CR=2.2; 5%wt. CaF$_2$; T=1000 °C] (a) Microprobe analysis at the surface of the alloy (b) SEM micrograph.

Figure 5:

Optical micrograph of a cross section of the Cu-Ni 55-45 alloy after electrolysis at E=1.80 V vs. AlF$_3$/Al for 800 s in the oxide-free cryolite melt [CR=2.2; 5%wt. CaF$_2$; T=1000 °C].

Figure 6:

Comparison of the steady state current versus potential curves (0.002 V s^{-1}) on copper and nickel in the alumina-containing cryolite melt [5wt%. Al$_2$O$_3$, CR=2.2; 5%wt. CaF$_2$; T=970 °C] and in the alumina-free melt [CR=2.2; 5%wt. CaF$_2$; T=1000 °C].

Figure 7:

Comparison of the steady state current versus potential curves (0.002 V s^{-1}) on 70-30 copper-nickel alloy in the alumina-containing cryolite melt [5wt%. Al$_2$O$_3$, CR=2.2; 5%wt. CaF$_2$; T=970 °C] and in the alumina-free melt [CR=2.2; 5%wt. CaF$_2$; T=1000 °C].

Figure 8:

Potentiostatic polarization (E=1.80 V vs. AlF$_3$/Al) on copper, nickel and copper-nickel 70-30 alloy in the alumina-containing cryolite melt [5wt%. Al$_2$O$_3$, CR=2.2; 5%wt. CaF$_2$; T=970 °C].

Figure 9:

Comparison of the open circuit potential recordings obtained on copper electrodes after a current pulse (5 s at 0,75 A cm^{-2}) in the alumina-free melt [CR=2.2; 5%wt. CaF$_2$; T=1000 °C] and in the alumina-containing melt [5wt%. Al$_2$O$_3$, CR=2.2; 5%wt. CaF$_2$; T=970 °C].

Figure 10:

Open circuit potential recordings on copper, nickel and copper-nickel 70-30 after a current pulse in the alumina-containing melt [5wt%. Al$_2$O$_3$, CR=2.2; 5%wt. CaF$_2$; T=970 °C].

Figure 11:

SEM-BSE micrographs of cross sections of copper and nickel electrodes after anodic polarization at E=1.80 V vs. AlF$_3$/Al for 100 s (Ni) and 200 s (Cu) in the alumina-containing melt [5wt%. Al$_2$O$_3$, CR=2.2; 5%wt. CaF$_2$; T=970 °C].

Figure 12:

Characterization of a cross section of a copper-nickel 70-30 electrode after anodic polarization at 1.50 V vs. AlF$_3$/Al during 1000 s in cryolite melt [CR = 2.2; 5%wt. CaF$_2$; 5%wt. Al$_2$O$_3$; T=970°C] (a) SEM-BSE micrograph (b) Microprobe determination of the molar fraction of Ni, Cu and O through the interface.

Figure 13:

Quantitative distribution of Cu, Ni, O and Al obtained by microprobe analysis of the cross section of the copper-nickel 70-30 alloy after polarization at 1.80 V vs. AlF$_3$/Al for 1800 s in cryolite melt [5wt%. Al$_2$O$_3$, CR=2.2; 5%wt. CaF$_2$; T=970 °C].

Figure 14:

SEM-BSE micrographs of cross sections of a copper and a copper-nickel electrode after electrolysis at 0.8 A.cm^{-2} during 500 s in cryolite melt [5wt%. Al$_2$O$_3$, CR=2.2; 5%wt. CaF$_2$; T=970 °C].

Table 1:

Dissolution potential of copper, nickel, 70-60 and 55-45 copper-nickel alloys measured in the oxide-free cryolite melt [CR=2.2; 5%wt. CaF_2; T=1000 °C].

Figure 1

16

Figure 2
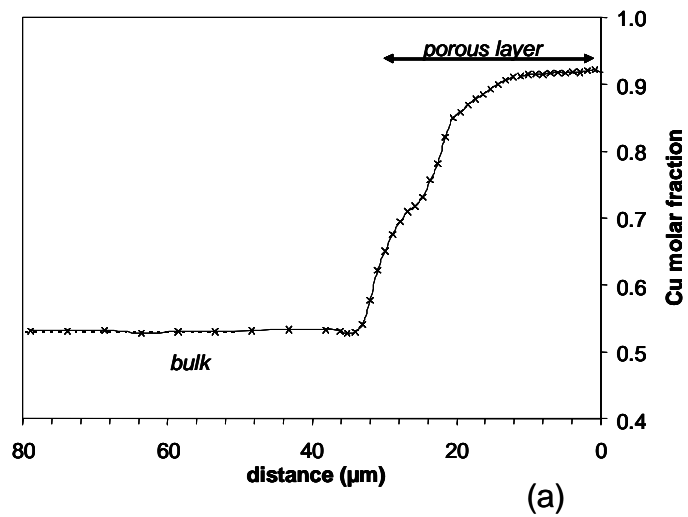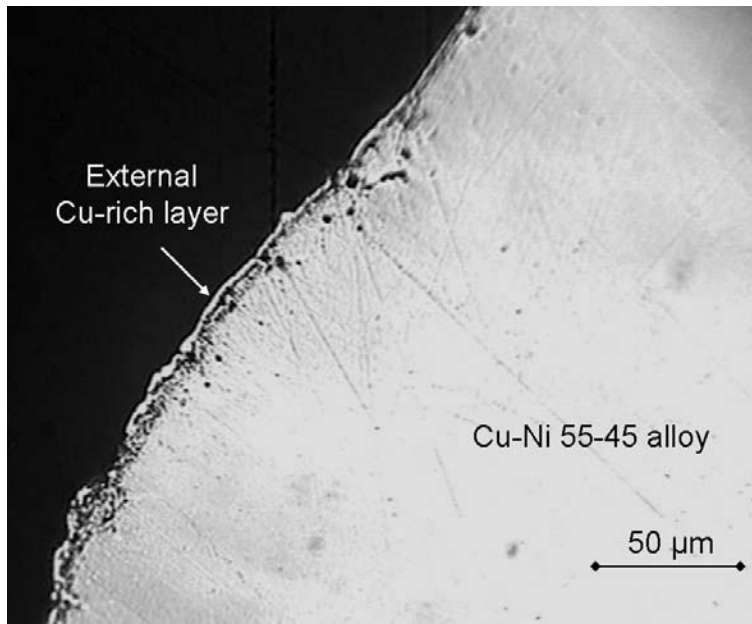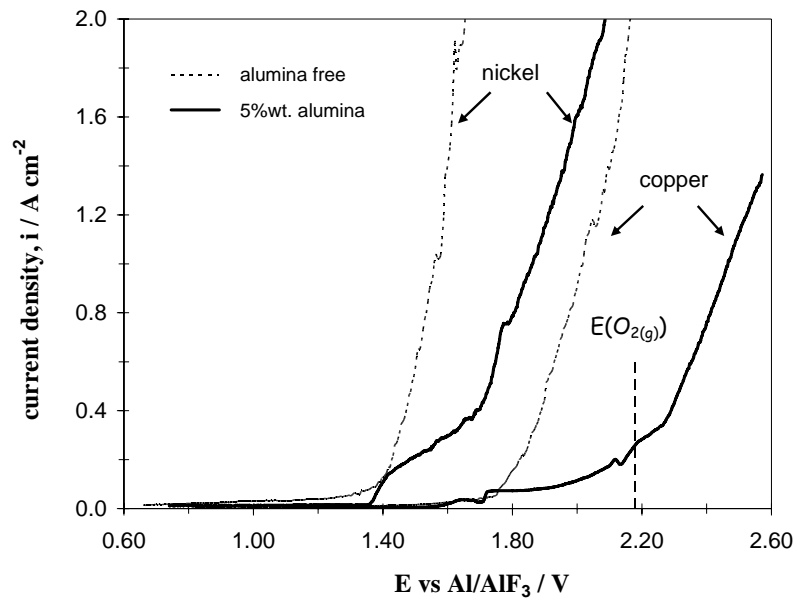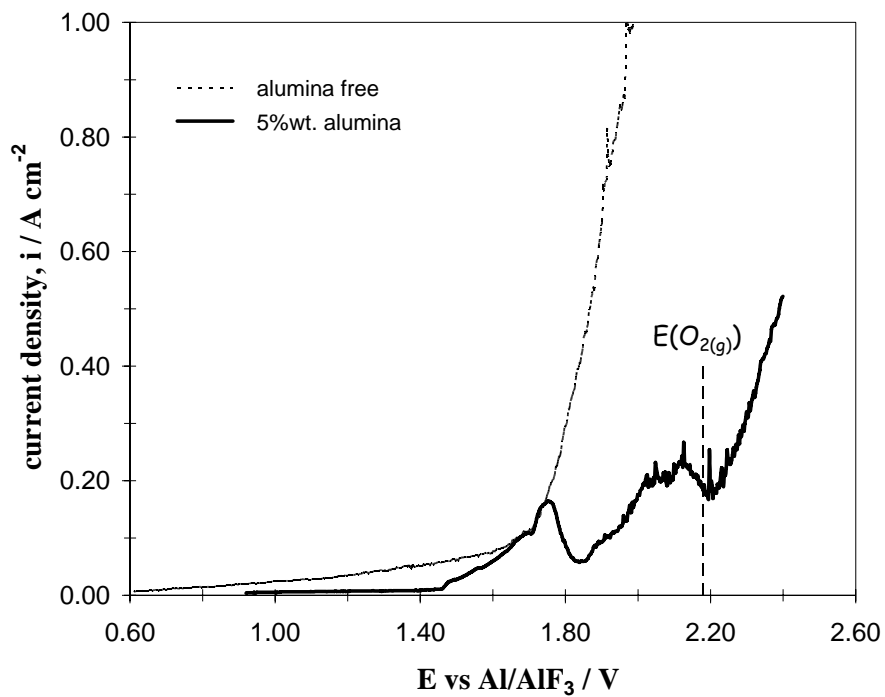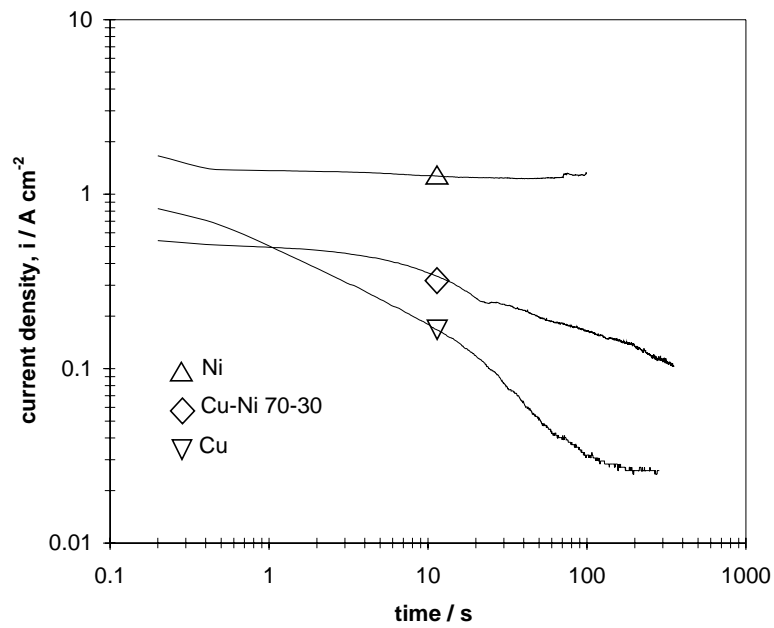
Figure 3

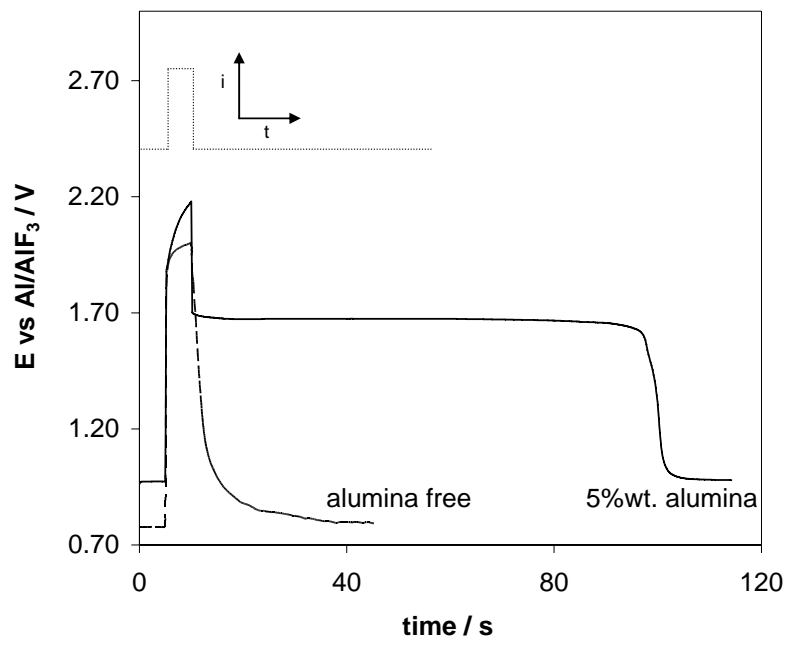Figure 4

External Cu-rich layer

Cu-Ni 55-45 alloy
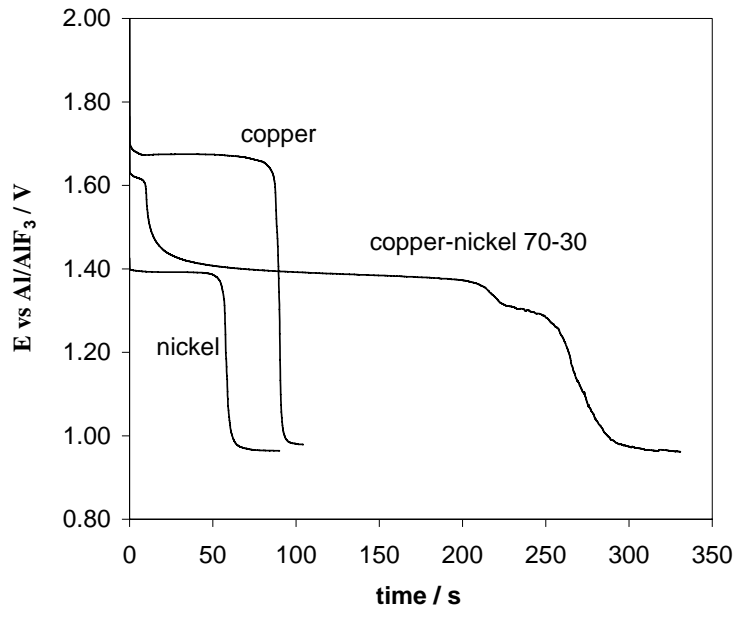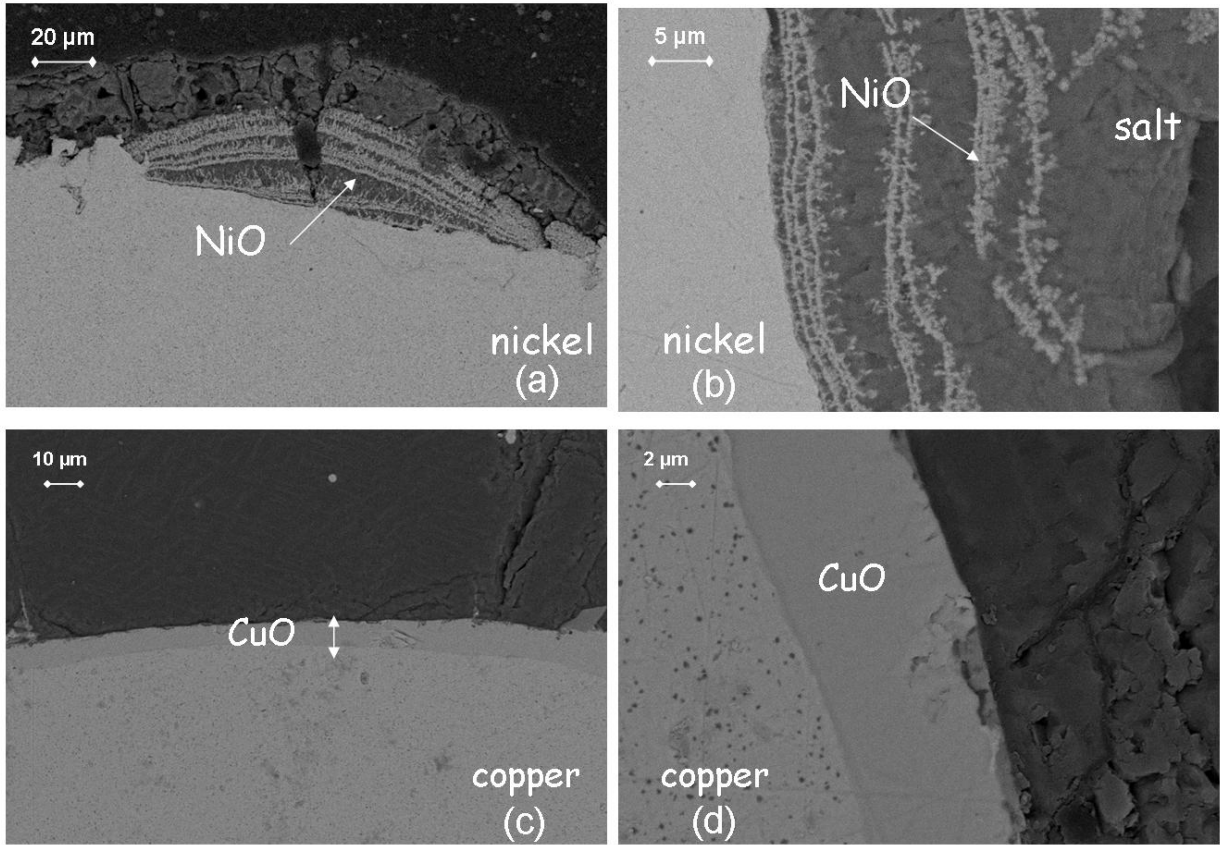
50 µm
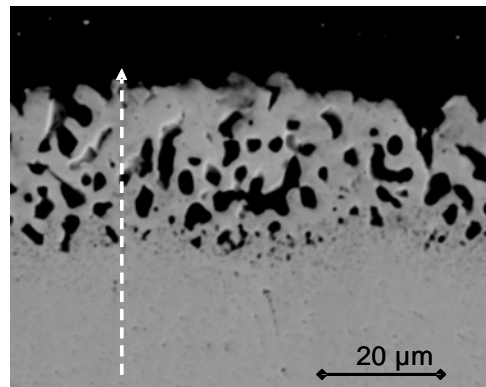
Figure 5

Figure 6
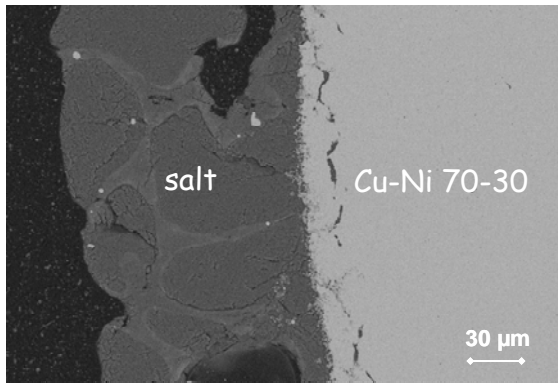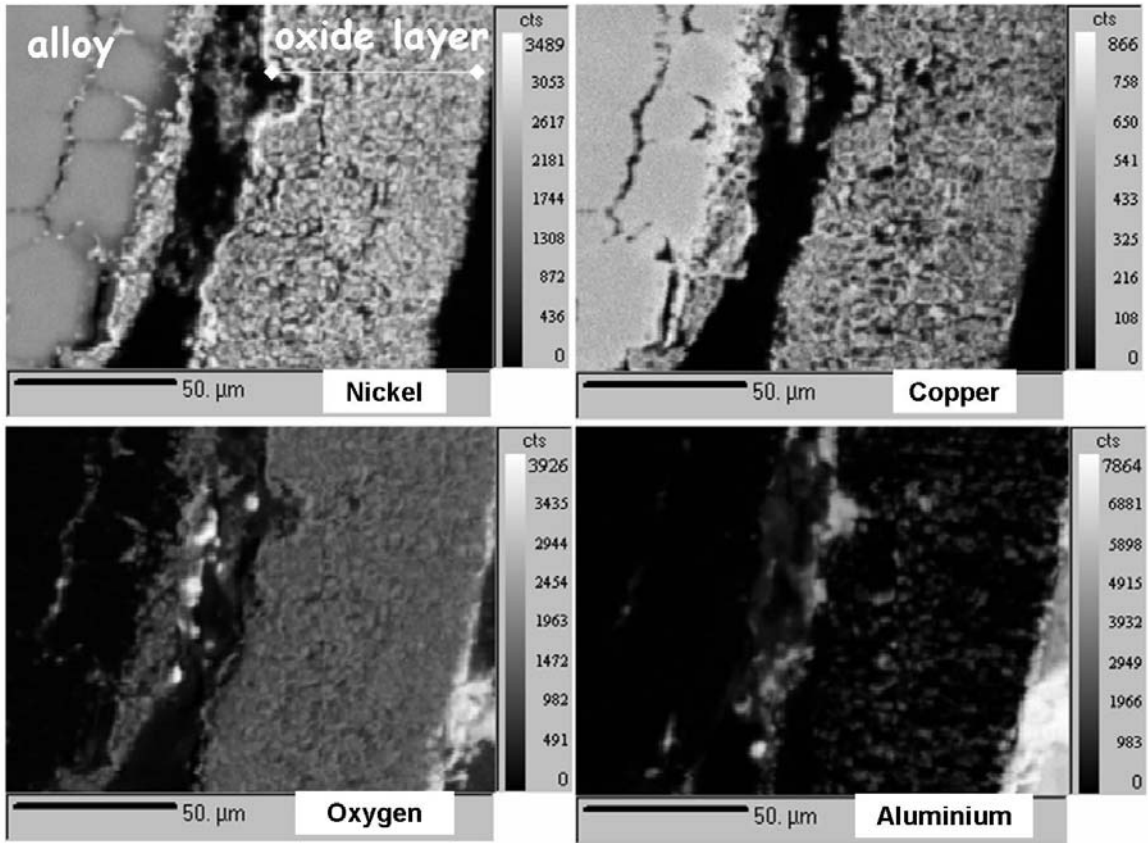
Figure 7

Figure 8

Figure 9

Figure 10

Figure 11
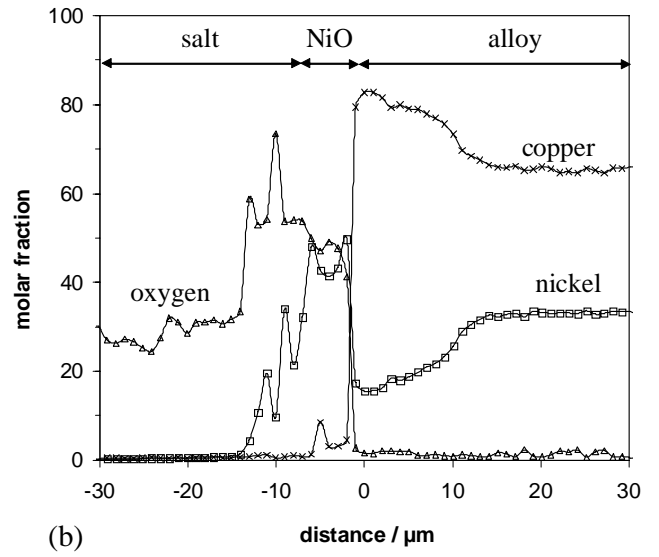
(a)   (b)

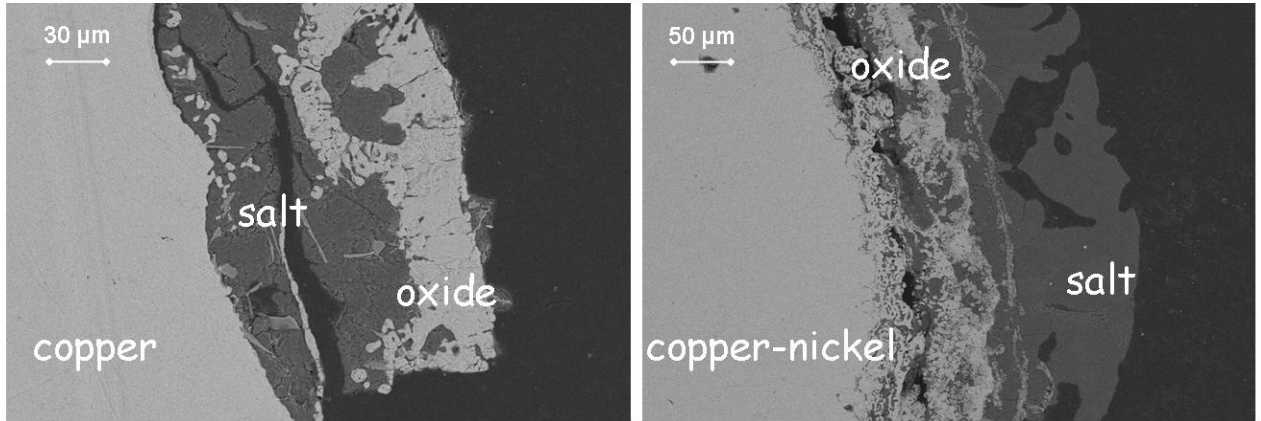Figure 12

Figure 13

Figure 14

Metal	Dissolution potential (vs Al/AlF$_3$) / V
Copper	1.75
Cu-Ni 70-30	1.65
Cu-Ni 55-45	1.50
Nickel	1.40

Table 1